The scaffolding and activation of NLRP3 on acidic vesicles depends on their biophysical properties and is independent of intermediate filaments

Guillermo de Paz Linares[1,2], Jan Mossemann[1], Blayne Sayed[1,3], and Spencer A. Freeman[1,2*]

[1]Program in Cell and Systems Biology, SickKids Research Institute, Toronto, Ontario M5G 0A4, Canada

[2]Department of Biochemistry and the [3]Institute of Medical Science, University of Toronto, Toronto, ON M5S 1A8, Canada.

*Corresponding author: spencer.freeman@sickkids.ca

Key words: vimentin, V-ATPase, LAMP1, PI(4)P, PI(3,5)P2, PI(3)P, membrane tension, membrane potential, ischemia reperfusion injury

Running title: Biophysical determinants of NLRP3 activation

Abstract

Inflammasomes are nucleated by receptors that become activated upon cellular stresses including ionic dyshomeostasis. Rather than forming in the cytosol, recent evidence suggests that inflammasomes are nucleated at specific sites in the cell including on cytoskeletal polymers and the membrane surfaces of organelles. The NLRP3 inflammasome, which is formed upon the loss of cytosolic K^+, had been proposed to form on intermediate filaments as well as on vesicles along the endocytic pathway. To determine the necessary requirement of either mechanism, we used vimentin knockout macrophages which do not have intermediate filaments and compared the formation and function of NLRP3 inflammasomes. We report that vimentin was dispensable for the activation of caspase-1, IL-1β cleavage and release, and inflammatory responses in mice attributed to the inflammasome. Instead, NLRP3 was recruited to PI(3,5)P2, PI(4)P- and LAMP1-positive compartments undergoing osmotic swelling. Swelling of these compartments was dependent on the V-ATPase, the inhibition of which curtailed NLRP3 recruitment and inflammasome activation. Similarly, decreasing the hydrostatic pressure on these vesicles prevented NLRP3 recruitment, IL-1β release and pyroptosis. The results suggest that NLRP3 is activated by biophysical features of acidic organelles in the endocytic pathway.

Introduction

Inflammasomes are supramolecular organizing centres that assemble in response to diverse threats to cell and tissue homeostasis. Such threats often involve the loss of membrane integrity and/or the breach of the cytosol by microbial-associated molecules (Greaney, Leppla, and Moayeri 2015). The damage that triggers inflammasome activation ultimately leads to cytokine processing and release, which in turn promotes inflammatory cascades and the recruitment of immune cells. Inflammasome assembly is a stepwise process which begins with a transcriptional 'priming' step that upregulates expression of its necessary components. This is followed by the sensing of intracellular perturbances via cytosolic pattern recognition receptors and their recruitment of the effector protease, caspase-1. Once concentrated, caspase-1 initiates autolytic cleavage/activation, and subsequent processing of inflammatory mediators including IL-1β and gasdermin D (Brough and Rothwell 2007; He et al. 2015). The NLRP3 inflammasome, which has been extensively studied, is activated in response to insults that ostensibly cause the collapse of the Na^+:K^+ gradient between the cytosol and the external medium (Muñoz-Planillo et al. 2013; Perregaux and Gabel 1994; Mangan et al. 2024). Its activation is therefore initiated upon increased permeability of the plasma membrane, which can occur following exposure to diverse bacterial toxins and damage-associated molecular patterns, like extracellular ATP (Franchi and Núñez 2008; Perregaux and Gabel 1994; Laliberte, Eggler, and Gabel 1999). The accumulation of damaging particulates in the endocytic pathway, including alum and monosodium urate crystals (MSU), also triggers NLRP3 inflammasome activation (Hanfen Li et al. 2008; Hornung et al. 2008; Martinon et al. 2006), though mechanisms in this case –and whether these converge on ionic homeostasis– are less clear (Mangan et al. 2024).

Pharmacology aimed at inhibiting NLRP3 has shown enormous potential in mitigating conditions with an underlying chronic inflammatory etiology (Hao Li et al. 2022). Despite the

translational relevance of NLRP3 nucleation, recent studies on the location of NLRP3 inflammasome assembly have been seemingly at odds with one another. One report by dos Santos et al., argued that vimentin-based intermediate filaments are required for the assembly of the NLRP3 inflammasome in primary murine macrophages (dos Santos et al. 2015). NLRP3 was found to colocalize and co-sediment with vimentin and the loss of vimentin prevented inflammasome assembly and inflammation. This would seem to be in contrast to other, subsequent reports (Chen and Chen 2018; Zhang et al. 2023; Schmacke et al. 2022) that have found that NLRP3 begins to aggregate on intracellular vesicles enriched for phosphatidylinositol-4-phosphate (PI4P). A stretch of cationic residues found in NLRP3 is thought to facilitate interactions with the negatively charged PI4P. This motif, known as the polybasic region, was essential in mediating the initial assembly of the NLRP3 inflammasome in cell lines (Chen and Chen 2018; Schmacke et al. 2022). Thus, the two models appear to be diametrically opposed, since vimentin is not known to be required for any PI4P-mediated processes.

In this report, we revisit the role of intermediate filaments in the inflammatory response of macrophages, where cytosolic intermediate filaments are solely comprised of vimentin, to NLRP3-activating stimuli. Despite reports of vimentin knockout (*Vim*$^{-/-}$) mice as being protected against a plethora of inflammatory insults (Jiang et al. 2012; dos Santos et al. 2015; Mor-Vaknin et al. 2013; Håversen et al. 2018), we do not find a role for vimentin in the nucleation of the NLRP3 inflammasome nor the subsequent release of inflammatory cytokines from macrophages. Supporting this, we found that *Vim*$^{-/-}$ mice were not protected against inflammation in an *in vivo* model of liver ischemia reperfusion injury (IRI), an NLRP3-dependent process (Wu et al. 2022). Therefore, it appears that the protective effects observed in *Vim*$^{-/-}$ mice are attributed to functions independent of NLRP3.

Instead, we find that NLRP3 is recruited to PI4P-, PI(3,5)P_2, and LAMP1-positive vesicles undergoing osmotic swelling that appear shortly after collapsing K^+ gradients. NLRP3

102 recruitment to vesicles (and the resultant IL-1β release) was reversed upon relieving their
103 hydrostatic pressure. Rather than swelling alone being a trigger of assembly, NLRP3
104 inflammasome activity was dependent on the V-ATPase, implicating K^+-H^+ transport on acidic
105 organelles. This suggests that underappreciated biophysical features and ion transport across
106 endomembranes play critical roles in triggering the formation of the NLRP3-inflammasome.
107

108 **Results**

109 *ASC specks form independently of vimentin*

110 To test the proposed requirement for vimentin filaments in the nucleation of the NLRP3
111 inflammasomes, we derived primary macrophages from the bone marrow of *Vim*$^{-/-}$ mice. Our
112 bone marrow-derived macrophages (BMDM) did not express vimentin as judged by western
113 blotting (**Fig 1A**) and immunofluorescence (**Fig 1B**). NLRP3-mediated pyroptosis is triggered by
114 the depletion of intracellular [K^+], including for primary macrophages (Muñoz-Planillo et al.
115 2013). Experimentally, this is most conveniently achieved with nigericin, a K^+ ionophore.
116 Alternatively, we also used ATP, which engages purinergic receptors to cause their
117 multimerization and formation of a non-selective pore that conducts K^+ down its concentration
118 gradient, i.e., out of the cell (Pelegrin and Surprenant 2006). We treated macrophages with
119 nigericin or ATP at standard concentrations and times known to instigate NLRP3 inflammasome
120 formation in a manner dependent on net K^+-efflux (Perregaux and Gabel 1994; Muñoz-Planillo
121 et al. 2013). Using atomic absorption spectroscopy, we found that the loss of intracellular K^+
122 upon the addition of nigericin or ATP was not different between wt and *Vim*$^{-/-}$ BMDM, as
123 expected **(Fig. 1C)**. Therefore, any differences in NLRP3 inflammasome activation would not be
124 caused by protection against intracellular [K^+] depletion in *Vim*$^{-/-}$ BMDM.

125 Next, we visualized ASC speck formation in lipopolysaccharide (LPS)-primed BMDM,
126 which upregulates the expression of NLRP3 (Bauernfeind et al. 2009), upon K^+ efflux. ASC is a
127 critical adaptor that enables the recruitment of caspase-1 to NLRP3 and its subsequent

128 activation (Man et al. 2014). We stained endogenous ASC following nigericin or ATP treatment
129 and, surprisingly, found no difference in the incidence of ASC-speck positive BMDM between wt
130 and *Vim*$^{-/-}$ cells **(Fig. 1D,E).** Even more remarkable, when analyzing images using a Pearson's
131 coefficient, we found there to be no correlation between the localization of vimentin intermediate
132 filaments and ASC specks following NLRP3 inflammasome activation **(Fig. 1F,G)**. This is
133 despite the fact that the intermediate filaments persisted in activated cells. Altogether, these
134 observations would seem to indicate that the assembly of the NLRP3 inflammasome is not
135 dependent on the presence of vimentin intermediate filaments.
136
137 *Vimentin is not required for NLRP3-mediated pyroptosis*
138 Once the NLRP3 inflammasome forms, active caspase-1 then cleaves gasdermin D
139 (GSDMD) and pro-IL-1β. Subsequently, the N-terminus of GSDMD inserts into the plasma
140 membrane to form a pore that allows for the passage and release of the processed (mature) IL-
141 1β (Evavold et al. 2018). The involvement of intermediate filaments in GSDMD pore assembly
142 was not assessed in previous studies; conceivably, if vimentin controlled the release of
143 proinflammatory mediators it would explain some results in mice in which KOs are protected
144 from inflammation (Jiang et al. 2012; Håversen et al. 2018; Mor-Vaknin et al. 2013; dos Santos
145 et al. 2015). We treated LPS-primed wt and *Vim*$^{-/-}$ BMDM with nigericin along with propidium
146 iodide (PI) in order to identify potential differences in the rate of plasma membrane
147 permeabilization **(Fig. 2A,B)**. However, we did not see appreciable differences between the
148 vimentin KO macrophages when compared to their wt counterparts.
149 Sustained GSDMD pore activity eventually leads to an irreversible form of lytic cell death
150 known as pyroptosis that further promotes IL-1β release into the interstitium (Fink and Cookson
151 2006; He et al. 2015). Thus, we investigated whether the absence of vimentin in BMDM could
152 prevent or stagnate pyroptosis by measuring the release of lactate dehydrogenase (LDH). In

153 addition to instigating pyroptosis with nigericin or ATP, we also employed alum and MSU crystals
154 to trigger the process. As shown by this assay, nigericin, ATP, alum, or MSU induce lytic cell
155 death in both wt and *Vim*$^{-/-}$ LPS-primed BMDM **(Fig. 2C)**. Moreover, the amount of LDH released
156 from *Vim*$^{-/-}$ BMDM was not significantly different than wt BMDM, irrespective of the NLRP3
157 inflammasome activator used. Based on our results, we conclude that *Vim*$^{-/-}$ BMDM are not
158 protected against pyroptotic cell death.
159
160 *Vimentin is not required for NLRP3-dependent cleavage and release of caspase-1 nor IL-1β*
161 During pyroptosis, caspase-1 activation precedes the cleavage of IL-1β and has been
162 reported to exit the cell as an active protease following cell rupture (Laliberte, Eggler, and Gabel
163 1999). Indeed, we found cleaved (i.e., active) caspase-1 in the supernatants of LPS-primed
164 BMDM that were treated with either nigericin or ATP **(Fig. 3A)**. Remarkably, we saw that *Vim*$^{-/-}$
165 BMDM were activating and releasing comparable amounts of caspase-1 compared to their wt
166 BMDM counterparts upon pyroptotic stimuli **(Fig. 3A,B)**. Ultimately, IL-1β is a major effector
167 cytokine that results in the propagation of inflammatory responses. We found that BMDM
168 derived from the *Vim*$^{-/-}$ mice had no impairment in the upregulation of pro-IL-1β upon LPS
169 stimulation **(Fig. 3C)** and released similar levels of active IL-1β into the supernatant after
170 stimulation with either nigericin or ATP **(Fig 3C)**. Furthermore, we saw no difference in the
171 mature IL-1β concentration found in the extracellular medium of LPS-primed BMDM treated with
172 nigericin or ATP, or upon lysosomal stress (i.e., alum or MSU) **(Fig. 3D)**. Overall, we did not
173 observe any impairment in capase-1 and IL-1β processing and release from *Vim*$^{-/-}$ BMDM.
174
175 *Vim*$^{-/-}$ *mice are not protected against hepatic ischemia/reperfusion injury*
176 Despite our *in vitro* observations, there is a plethora of studies reporting that *Vim*$^{-/-}$ mice
177 display reduced tissue damage upon numerous inflammatory stimuli (Jiang et al. 2012;

178 Håversen et al. 2018; Mor-Vaknin et al. 2013). In fact, others have reported that *Vim*$^{-/-}$ mice are
179 protected against cerebral IRI (Jiang et al. 2012). Thus, we probed whether this protection
180 translated to a hepatic IRI model, which is reportedly mediated, at least in part, by NLRP3
181 (Jaeschke 2003; Jiménez-Castro et al. 2019; Zhu et al. 2011). Following 1 h of ischemia and 6 h
182 blood reperfusion, we collected samples from mice to look at different aspects of inflammatory
183 injury. First, we did not observe any cohort differences in plasma levels of liver enzymes alanine
184 aminotransferase (ALT) and aspartate aminotransferase (AST) **(Fig. 4A,B)**, indicating that liver
185 damage was not ameliorated in the absence of vimentin. Our histological analyses in which we
186 categorized the percentage of necrotic tissue found in the livers after surgery (*see demarcated*
187 *yellow areas in* **Fig. 4C**) revealed that, surprisingly, *Vim*$^{-/-}$ livers were more necrotic compared to
188 wt **(Fig. 4D)**. Based on these observations, we conclude that the absence of vimentin does not
189 confer a protective effect against the inflammatory damage associated with hepatic IRI.
190
191 *NLRP3 is recruited to PI4P- and PI(3,5)P_2-containing vesicles*
192 An opposing view to the role of intermediate filaments in scaffolding the NLRP3
193 inflammasome is that the complex is instead assembled on vesicular membranes requiring
194 electrostatic interactions between NLRP3 and phosphoinositides (Schmacke et al. 2022; Chen
195 and Chen 2018; Zhang et al. 2023). NLRP3 is reported to recognize PI3P, PI4P, and PI(3,5)P_2 *in*
196 *vitro*, though only its interaction with PI4P has been demonstrated in cells (Chen and Chen
197 2018). We therefore expressed an mCherry-NLRP3 fusion protein in HeLa cells, noting that
198 nigericin treatment resulted in its clear enrichment at vesicular structures over the course of 1
199 hour **(Fig. 5A and Supplemental movie 1)**. Using biosensors for relevant phosphoinositides,
200 we reperformed this experiment and used Statistical Object Distance Analysis (SODA) to
201 determine coincidence of the signals, which provides statistical maps of the assemblies in a
202 population of objects by using morphology and the distance separating objects (Lagache et al.
203 2018). By this method, we identified objects that were significantly coupled at a radius of 6

204 pixels from each object centre. We noted no appreciable association between NLRP3 and PI3P
205 (PX-GFP) both at 15 min and at 1 hour **(Fig. 1S)**. Interestingly, by using a recently developed
206 probe for PI(3,5)P_2, SnxA-GFP, we found clear association between NLRP3 and PI(3,5)P_2 15
207 min post nigericin treatment **(Fig. 1S)**. The association between NLRP3 and PI4P (GFP-P4M)
208 was higher and followed a similar trend to that of PI(3,5)P_2. As the vesicles increased in size
209 over time, we noted less enrichment of the phosphoinositides on these compartments, which
210 would be consistent with defects in membrane traffic likely occurring well after NLRP3
211 activation. These data corroborate the finding that NLRP3 assembly is, initially, spatially
212 organized around sites of enriched with PI4P and reveal the possibility that PI(3,5)P_2 plays a
213 role in NLRP3 activation.
214
215 *Nigericin causes the swelling of LAMP1-positive vesicles that recruit NLRP3*
216 To further characterize the relevant organelle(s) that recruit NLRP3, we co-expressed
217 mCherry-NLRP3 together with early endosomal (GFP-EEA1) and late endosomal (LAMP1-
218 mEmerald) markers. The same SODA analysis was applied which revealed that NLRP3
219 associates preferentially with LAMP1-positive vesicles following loss of cytosolic potassium
220 **(Fig. 5B,C)**. This association was present at both 15 min and 1 h post nigericin treatment. As
221 with PI(4)P and PI(3,5)P_2, we noticed that the association of NLRP3 with LAMP1 vesicles once
222 they were swollen tended to be 'low' for their expression of LAMP1 while less swollen
223 compartments that associated with NLRP3 were 'high' for LAMP1 expression. At later timepoints
224 (i.e., 1 h) NLRP3 associated exclusively with swollen, 'low' LAMP1 membrane-bound
225 compartments. This could either reflect the extent to which these vesicles had undergone
226 swelling or the nature of the compartment itself. In contrast, we did not see appreciable NLRP3
227 aggregation on EEA1-positive compartments at either timepoint. This would suggest that an
228 initiating event in NLRP3 activation occurs at vesicular compartments containing LAMP1 that
229 are beginning to undergo swelling.

230

231 *Increases in hydrostatic pressure and the V-ATPase are required for NLRP3 inflammasome*

232 *assembly and IL-1β release*

233 Swelling of organelles in the endocytic pathway alone would seem unlikely to activate

234 NLRP3; lysosomal storage disorders or osmotic imbalances of endolysosomes do not lead to

235 IL-1β release or pyroptosis (Cai et al. 2024). Supporting this, incubation of cells with a non-

236 digestible, non-transportable disaccharide, sucrose, did not lead to the vesicular recruitment of

237 NLRP3 or pyroptosis, despite leading to the swelling of LAMP1 positive compartments **(Fig.**

238 **6A,C).** Vesicular swelling may nevertheless be required for NLRP3 recruitment. To test this, we

239 prevented the gain in hydrostatic pressure incurred upon nigericin treatment by shifting the cells

240 to hypertonic solutions at the time of its addition. The increase in extracellular osmolarity causes

241 water to leave the cell, and organelles, concomitantly (Lang et al. 1998; Hohmann 2002). Under

242 such conditions, we saw the expected inhibition of vesicular swelling. Importantly, preventing the

243 gain in hydrostatic pressure eliminated the recruitment of NLRP3 to vesicular compartments.

244 Instead, NLRP3 remained largely soluble **(Fig. 6B)** and pyroptosis as well as IL-1β release were

245 averted in BMDM **(Fig. 6C,D)**.

246 The swelling caused by nigericin, a membrane-permeable ionophore, may be owed to its

247 direct targeting of endomembranes. Once inserted into the limiting membrane of acidic

248 organelles, nigericin would serve to exchange H^+ for K^+, the latter of which may drive swelling. If

249 this is the case, inhibition of the H^+ gradient (by first inhibiting the V-ATPase) would prevent the

250 accumulation of K^+. We therefore inhibited the V-ATPase with concanamycin A prior to nigericin

251 addition. This treatment prevented the swelling of LAMP1-positive structures. Critically, this

252 treatment also prevented the recruitment of NLRP3 **(Fig. 6B).** Moreover, concanamycin A pre-

253 treatment led to a reduction in pyroptosis and IL-1β release in LPS-primed BMDM after nigericin

254 addition **(Fig. 6C,D)**. Taken together, we conclude that vesicles endowed with active V-ATPases
255 are the sites of NLRP3 scaffolding and activation upon disruptions to organellar ion transport.
256
257 **Discussion**
258 NLRP3 plays a crucial role by acting as a sensor of intracellular dyshomeostasis to then
259 invoke inflammation. K^+ efflux, indicative of lost plasma membrane integrity or inhibition of the
260 Na^+/K^+-ATPase, is a major trigger of NLRP3 inflammasome assembly (Muñoz-Planillo et al.
261 2013). Solid particles/crystals also activate the NLRP3 inflammasome by causing stress and
262 dysregulation along the endocytic pathway (Hanfen Li et al. 2008; Hari et al. 2014; Groß et al.
263 2016; Hornung et al. 2008). Whether or not these two, seemingly different stimuli converge
264 mechanistically has not been clear, but this is discussed later on below. Rather than directly
265 sensing differences in alkali cation (Na^+, K^+) concentrations in the cytosol, disruption of their
266 normal gradients leads to changes in the cell which are then sensed by NLRP3.
267 In this study, we demonstrate that vimentin is dispensable for NLRP3-inflammasome
268 assembly and instead find that the V-ATPase and vesicular swelling are required. While many
269 studies implicate vimentin in inflammatory cascades (Mor-Vaknin et al. 2013; Jiang et al. 2012;
270 Eckes et al. 2000; Håversen et al. 2018), this may be owed to impaired immune cell migration
271 and infiltration to inflamed tissues (Barberis et al. 2009; Battaglia et al. 2018; Ivaska et al. 2007;
272 Nieminen et al. 2006). In line with other studies (Zhang et al. 2023; Chen and Chen 2018), our
273 data show that the formation of NLRP3 inflammasomes occurs at vesicular sites enriched in
274 PI4P and, interestingly, $PI(3,5)P_2$. Normally these lipids are found in compartments that are
275 distinct from one another, which could be the case here as well since we were not able to image
276 both PIPs together with NLRP3. Alternatively, the immediate impact that nigericin has on
277 membrane traffic could cause the loss of organellar identity in the cells, causing these PIPs to
278 be on the same compartment.

279 PI4P has recently been shown to mediate other important immune processes pertaining
280 to intracellular danger signals. The cGAS-STING pathway, responsible for sensing cytosolic
281 DNA, was shown to be affected by changes to the intracellular pool of Golgi-PI4P and its
282 associated kinase, PI4KB (Fang et al. 2023; Luteijn et al. 2024). This suggests that the
283 availability of PI4P plays broad and diverse roles in facilitating innate immune responses. Under
284 normal conditions, the majority of PI4P is in the Golgi apparatus and the plasma membrane, as
285 tightly regulated by lipid kinases and phosphatases (Tan and Brill 2014). Nucleation of the
286 inflammasome does not occur at these sites, suggesting that while PI4P may be an essential
287 component of NLRP3 inflammasome activation, there are likely coincidently detected
288 determinants in vesicles that recruit the receptor. The location of PI4P to compartments in which
289 it is not normally found may therefore be an important trigger of inflammation. In contrast to
290 PI4P, little is known about roles for PI(3,5)P_2 in innate immune sensing and signaling. Lipid-
291 protein overlay assays previously found that NLRP3 can bind PI(3,5)P_2 (Chen and Chen 2018),
292 though the importance of this interaction remains to be tested.
293 Others have reported that NLRP3 can bind to vesicles along the endocytic pathway
294 marked with EEA1, Rab5, and/or LAMP1 (Lee et al. 2023; Zhang et al. 2023). We found NLRP3
295 to preferentially associate with swollen, LAMP1-low vesicles and smaller, LAMP1-high vesicles
296 shortly after nigericin treatment, with this association shifting towards the former over the course
297 of an hour. The nature of these compartments is not yet known. What is clear is that the initial
298 acidification of these vesicles is required for the recruitment of NLRP3. Importantly, dissipation
299 of the H^+ gradient needs to occur <u>before</u> the addition of nigericin to prevent NLRP3 activation,
300 suggesting that the activity of the V-ATPase is not directly sensed by NLRP3. Nigericin acts as
301 an ionophore for H^+/K^+; its insertion into the plasma membrane drives K^+ loss for H^+ gain which
302 is an electroneutral process. Acidosis of the cytosol is then relieved by Na^+/H^+ exchangers,
303 causing the cell to gain Na^+. The ionophore also readily inserts into the membranes of
304 organelles. In acidic organelles, the driving forces for ion transport are entirely different from that

305 of the plasma membrane; here, H^+ will exchange for K^+ and drive K^+ into the lumen. In addition
306 to the swelling caused, this also has implications for the electrical potential of the membrane. It
307 is therefore possible that electrical, in addition to biophysical properties of the organelle, are
308 then sensed by NLRP3. While K^+-efflux is a common trigger of the NLRP3 inflammasome,
309 agents that damage lysosomes and/or disrupt endosomal traffic such as alum, monosodium
310 urate crystals, and silica particles also trigger its assembly (Hari et al. 2014; Groß et al. 2016).
311 Whether or not these damaging agents have similar effects on these electrical/biophysical
312 parameters warrants systematic inquiry.
313
314
315 **Methods and materials**
316 *Animals*
317 *Vim*$^{-/-}$ (129S-*Vim*^{tm1Cba}/MesDmarkJ, stock #025692) and wt 129S1 mice (129S1/SvImJ,
318 strain #002448) were obtained from Jackson Labs as previously described (Colucci-Guyon et al.
319 1994). C57Bl/6 wt mice from Jackson Labs (strain #000664) were used where indicated. All
320 procedures were approved by the Animal Care Committee at the Hospital for Sick Children and
321 were performed in accordance with regulations from the Animals for Research Act of Ontario
322 and the Canadian Council on Animal Care. Mice were kept at the Animal Facility in the Peter
323 Gilgan Centre for Research and Learning.
324
325 *Liver ischemia/reperfusion surgery*
326 Cohorts of 8- to 12-week-old Vimentin knockout and wt (C57Bl/6) control mice were
327 used in a 70% segmental warm ischemia-reperfusion model (Selzner et al. 2003). In brief, a
328 sagittal midline laparotomy was made under isoflurane anesthesia, and an atraumatic vascular
329 clamp was placed on the portal vein and the hepatic artery to block blood flow to the left and
330 medial lobes of the liver which account for about 70% of the liver parenchyma. The clamp was

331 removed after 1 h to allow for reperfusion. Following 6 h of reperfusion, mice were euthanized
332 before blood and tissue collection for analysis. Male mice were used to control for known sex
333 differences in IRI responses (W. Li et al. 2018; Ostadal et al. 2019).
334
335 *Reagents*
336 Mammalian expression vectors were obtained from the following sources: 2xSidM-GFP
337 as described in (Levin et al. 2017); pCAG mEmerald-LAMP1 was a gift from Franck Polleux
338 (Addgene plasmid # 168513); Human NLRP3 from pEGFP-C2-NLRP3 (gift from Christian
339 Stehlik, Addgene plasmid # 73955) was inserted into an mCherry-C2 mammalian vector by
340 Gibson assembly cloning (NEB, cat #E2611S); pJSK659 (SNX-A-GFP) was a gift from Jason
341 King (Addgene plasmid # 205128); and GFP-EEA1 was a gift from Silvia Corvera (Addgene
342 plasmid # 42307). Primary antibodies used were rabbit anti-cleaved caspase-1 (Asp296)
343 (E2G2I) (Cell Signaling, cat #89332), mouse anti-ASC (BioLegend, cat #676502), rabbit anti-
344 vimentin (Cell Signaling, cat #5741), rabbit anti-pro caspase-1 + p10 +p12 (Abcam, cat.
345 #ab179515) and rabbit anti-GAPDH (Cell Signalling, cat #2118S). Primary antibody validation
346 was done by western blot. Secondary antibodies conjugated with AlexaFluor-405, -488, -555, -
347 647 and donkey anti-goat HRP secondary antibodies were obtained from Jackson
348 ImmunoResearch. Secondary mouse and rabbit antibodies conjugated with HRP were obtained
349 from Cell Signaling.
350 Cell culture reagents used include Dulbecco's modified eagle medium (DMEM, Wisent,
351 cat. #319-007-CL), fetal bovine serum (Atlanta Biologicals, cat. #S12450), Gibco™ DMEM, high
352 glucose, HEPES, no phenol red (FischerScientific, cat. #21063029), HBSS w/out phenol red,
353 calcium and magnesium, supplemented with FBS (Wisent, cat. #311-512 CL**),** 100x antibiotic-
354 antimycotic solution (Wisent, cat. #450-115-CL), FuGENE 6 Transfection reagent (Promega,
355 cat. #E2691), phosphate buffered saline (Wisent, Sigma-Aldrich, cat#311-010-CL), nigericin
356 sodium salt (Cayman chemicals, cat. #11437), adenosine triphosphate (pH=7.4, cat. #A2383-

357 5G), propidium iodide (Invitrogen, cat. #P1304MP), alum hydroxide (Invivogen, cat. #21645-51-
358 2), monosodium urate crystals (Invivogen, cat. #1198-77-2), lipopolysaccharide (Sigma-Aldrich,
359 cat. # L9764-5MG), concanamycin A (Cayman, cat. # 11050), Prolong Gold Mounting medium
360 with DAPI (Invitrogen, cat #P36935). .
361
362 *Cell culture*
363 Bone marrow derived macrophages from the long bones of 6-12-wk-old wt and *Vim*$^{-/-}$
364 mice was harvested by centrifugation and grown in DMEM + 10% FBS + 10% L929 conditioned
365 medium containing macrophage colony stimulating factor (MCSF) + 1% penicillin-streptomycin
366 at 37°C and under 5% CO_2. Cells were used 5-7 days after isolation. HeLa cells were grown
367 and passaged in DMEM + 5% FBS + 1% penicillin-streptomycin at 37°C and 5% CO_2.
368
369 *Transfections*
370 HeLa cells were seeded on top of coverslips in 12-well plates and left to attach overnight
371 at 37°C and 5% CO_2. FuGENE6 Transfection reagent was added to room temperature serum-
372 free DMEM for 5 min, and then plasmid DNA was added at a 1:3 ratio of DNA (μg) to FuGENE6
373 (μL). Mixture was incubated at room temperature for 15 min and added to each well. Media was
374 changed 4 h post-transfection. Cells were transfected at ~60% confluency and incubated for at
375 least 18 h at 37°C and under 5% CO_2 after transfection.
376
377 *Intracellular [K^+] measurements*
378 BMDM were grown to 90% confluency in 2 separate 6-well plates with DMEM
379 supplemented with 10% FBS and 10% MCSF. Following nigericin or ATP stimulation, BMDM
380 from one plate were washed 3x in 150 mM LiCl (pH=7.4) and lysed in 5 mM HNO_3. Cell lysates
381 were incubated at 4°C overnight and centrifuged at 12,000 g for 15 min to remove any debris.

382 Samples and standards of known [K^+] were analyzed using a PinAAcle 900T Atomic Absorption
383 Spectrometer (PerkinElmer, Waltham, MA, USA) to assess the total amount of K^+ ions. In
384 parallel, BMDM from the second plate were washed as previously described and lifted in
385 isotonic solution. Cell concentration and volumes were determined electronically using a Z2
386 Coulter particle count and size analyzer (Beckman Coulter) to calculate total cell number and
387 volume for each sample. Intracellular concentrations of K+ were calculated by dividing the total
388 ion content by the total cell volume of each well.
389
390 *Immunostaining*
391 BMDM were grown to 70-80% confluency in 12-well plates with DMEM supplemented
392 with 10% FBS and 10% MCSF. Then, BMDM were primed with LPS (1 μg/mL, 4 h) and
393 subsequently treated with nigericin (10 μM, 30 min) or ATP (3 mM, 1 h). Cells were then fixed
394 with 4% PFA for 15 min, permeabilized in 0.1% triton for 5 min and blocked in 5% BSA
395 overnight. Primary and secondary antibodies were diluted to 1:100 and 1:500 in 2.5% BSA in
396 PBS, respectively, and added to coverslips at room temperature for 1 h. Coverslips were
397 washed 3 times with PBS following incubation. Slides were mounted using mounting media
398 containing DAPI.
399
400 *PI assay*
401 BMDM were grown to 70-80% confluency in 12 well plates with DMEM supplemented
402 with 10% FBS and 10% MCSF. Cells were primed with LPS (1 μg/mL) for 4 h before
403 simultaneously adding nigericin (10 μM) and propidium iodide (0.3 μg/mL). Pictures of each well
404 were taken in both brightfield and RFP setting of an EVOS microscope (ThermoFischer). At
405 least 3 images of different fields of view were obtained per well per timepoint. Quantification of
406 PI positivity was done in ImageJ using the “Cell counter” feature.

407

408 *LDH assay*

409 Cells were grown to 80-90% confluency in 12 well plates with DMEM supplemented with
410 10% FBS and 10% MCSF. Priming with LPS (1 μg/mL) was done for 4 h, then cells were treated
411 with nigericin (10 μM) for 30 min, ATP (3 mM) for 1 h, alum (100 μg/ml) for 6 h, or MSU (100
412 μg/ml) for 16 h in 0.1% FBS DMEM. The supernatants of each well were collected and
413 centrifuged at 13,000 g for 5 min, and cells in each well were washed with 1x PBS and lysed in
414 RIPA buffer with protease inhibitor. LDH release was assayed according to manual instructions
415 (CyQUANT LDH Cytotoxicity Assay, Invitrogen, cat #C20301).

416

417 *Western blotting*

418 BMDM were grown to 80-90% confluency in 6 well plates with 10% FBS and 10%
419 MCSF. Cells were primed with LPS (1 μg/mL) for 4 h, then treated in reduced serum medium
420 (0.1% FBS) with either nigericin (10 μM) for 30 min or ATP (3 mM) for 1 h. Supernatants were
421 prepared following the TCA precipitation protocol from (Volchuk et al. 2020). Briefly, samples
422 were centrifuged at 13,000 g for 5 min at 4°C to remove any debris and precipitated using 100%
423 TCA. Samples were then washed with ice cold acetone, then heated at 95° C, and finally
424 resuspended in 2x SDS-PAGE sample buffer. For the cell lysates, cells were washed with 1x D-
425 PBS and lysed with RIPA buffer with protease inhibitors. Lysates were centrifuged at 12,000 g
426 for 15 min at 4°C and prepared after determining protein concentration by BCA assay. Lysate
427 proteins were resolved in a 12% SDS-PAGE gel and supernatant proteins using a 15% SDS-
428 PAGE gel. Proteins were transferred to a PVDF membrane and immunoblotted with the
429 appropriate antibodies. Images were analyzed using ImageJ to determine the adjusted mean
430 gray intensity value of each band over the same area.

431

432 *IL-1β Enzyme linked immunosorbent assay (ELISA)*

433 BMDM were grown on 12-well plates to 80-90% confluency using DMEM supplemented
434 with 10% FBS and 10% MCSF. BMDM were stimulated and supernatants were collected and
435 centrifuged for 15 min (13,000 rpm, 4°C). Samples were diluted at a ratio of 1:5 of supernatant
436 to the provided dilution buffer. ELISAs were performed according to the manufacturer's
437 instructions (Mouse IL-1 beta ELISA kit, Abcam, cat. #ab100705). Sample absorbance was read
438 using a Varioskan LUX Plate Reader 1 w/Dual Injectors (Thermofischer Scientific)

439

440 *Microscopy*

441 Cells immunostained for ASC and vimentin, as well as live cell imaging was performed
442 by confocal microscopy using a spinning-disk Zeiss Axiovert 200 M microscope (Quorum
443 Technologies Inc.) with an ORCA-Fusion BT cMOS camera, and a five-line laser module with
444 405-, 443-, 491-, 561-, and 655-nm lines. The microscope operating software was Volocity v6.3
445 (Perkin Elmer). Images were acquired as Z-stacks with a 63×/1.4 NA for Vimentin/ASC images
446 and 25x/0.8 NA water objective for ASC-speck quantification images. For video acquisition of
447 NLRP3-expressing HeLa cells, a Zeiss Axio Observer microscope with a PCO camera and four-
448 line laser module with 405-, 443-, 491-, and 561-nm lines was used.

449 For live cell microscopy, coverslips were placed in a chamber with HBSS and imaged on
450 a pre-warmed stage and 63×/1.4 NA oil objective to 37° C. Coverslips used to acquire movies
451 were placed in a chamber along with phenol red-free DMEM and an environmental control
452 chamber set to 37° C and 5% CO_2. Movies were acquired as single-slice images over the
453 course of one hour.

454

455 *Image analysis*

456 Liver tissue was fixed in PFA and stained with hematoxylin and eosin. Slides were
457 digitalized and ischemic score was determined using the DenseNetV2 identifier available in the
458 HALO software. ASC-speck positivity and Pearson's correlation analysis were done using the
459 Volocity software over the ROI of individual cells. Pearson's correlation image thresholding was
460 done according to the (Costes et al. 2004) thresholding method to avoid any bias.
461 SODA analysis of HeLa cells expressing mCherry-NLRP3 and different probes was done
462 using the free image analysis software called Icy (http://icy.bioimageanalysis.org/) and using a
463 modified protocol from (Lagache et al. 2018). Briefly, detection of bright spots on single slice
464 two-channel images was calibrated using the Wavelet Spot Detector. Then, ROIs were made for
465 each individual cell and the statistical probability that spots from both channels were associated
466 with each other by random chance was calculated (as defined by $p > 0.05$). Probability was
467 found for different radii (*r)* distances from the centre of each spot. Represented in our figure is
468 the coupled puncta of NLRP3 within $r = 6$ pixels (~516 nm). For each biological replicate, 5-10
469 cells were analyzed using SODA per probe used.
470
471 *Data analysis*
472 All experiments and data were conducted with at least 3 biological replicates. Data is
473 represented as mean ± SEM or individual replicate values ± SD. Statistical significance was
474 determined using two-tailed unpaired Student's *t* test (significant difference threshold $p < 0.05$).
475 For multiple comparisons, two-way ANOVA was used with Tukey's correction for all wt vs *Vim*$^{-/-}$
476 analysis. All other multiple comparisons were done using a one-way ANOVA with Tukey's
477 correction. All experiments shown were conducted at least 3 independent times ($N \geqslant 3$). All data
478 analysis was done using GraphPad Prism 6 and Excel.
479
480

481 **Figures**

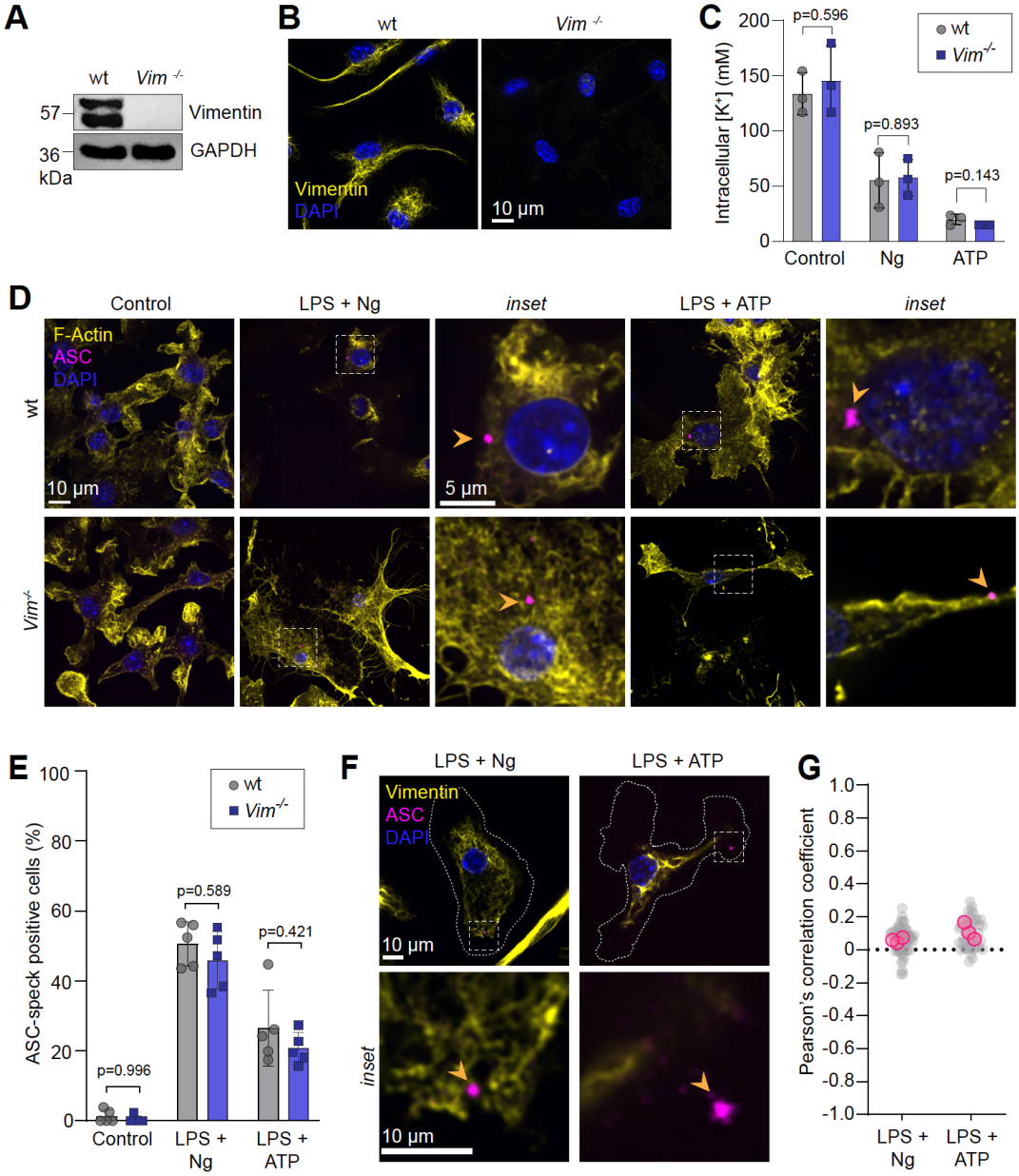

482

483 **Figure 1.** K^+-dependent ASC aggregation remains unaffected by the absence of vimentin
484 intermediate filaments. Validation of *Vim*$^{-/-}$ BMDM by A) western blot and B) vimentin
485 immunostaining as compared to wt control BMDM. (C) Intracellular K^+ concentration
486 measurements of BMDM following treatment with nigericin for 15 min or ATP for 30 min. Replicate
487 values ± SD are shown (N=3). (D-G) wt and *Vim*$^{-/-}$ BMDM primed with LPS (1 µg/mL, 4 h) and
488 treated with nigericin (10 µM, 30 min) or ATP (3 mM, 1 h). In (D,E), ASC was immunostained in
489 wt and Vim$^{-/-}$ BMDM, along with F-actin (phalloidin) and DAPI. Representative images shown in
490 D). Data are shown as mean of each replicate ± SEM in E (N=5). In (F,G) cells were
491 immunostained for vimentin and ASC in wt and *Vim*$^{-/-}$ BMDM. Representative images shown in F).
492 (G) Pearson's correlation coefficient per cell, grey dots and mean, pink dots (N=3, minimum 7
493 cells per replicate).

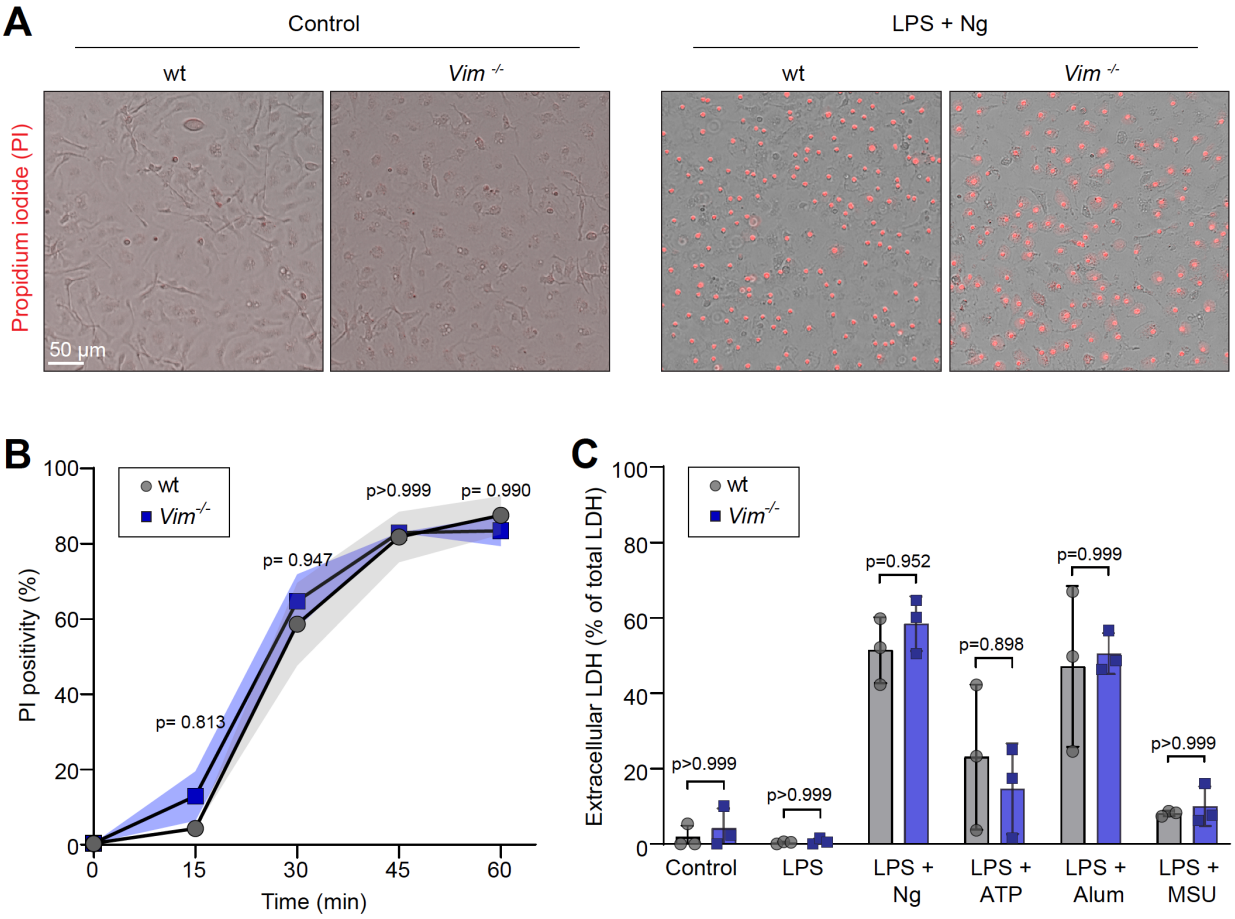

Figure 2. Pyroptotic cell death downstream of NLRP3 inflammasome activation is not dependent on vimentin intermediate filaments. (A,B) LPS-primed (1 μg/mL, 4 h) wt and *Vim*$^{-/-}$ BMDM stained with propidium iodide (1 μg/mL) after nigericin treatment (10 μM) over 1 h. Percent PI positivity is displayed in B) as the mean ± SEM of each timepoint. (N=3). (C) LDH release in wt and *Vim*$^{-/-}$ BMDM primed with LPS (1 μg/mL, 4 h) and treated with nigericin (10 μM) for 30 min, ATP (3 mM) for 1 h, alum (100 μg/ml) for 6 h, or MSU (100 μg/ml) for 16 h. Data represented as replicate mean ± SD (N=3)

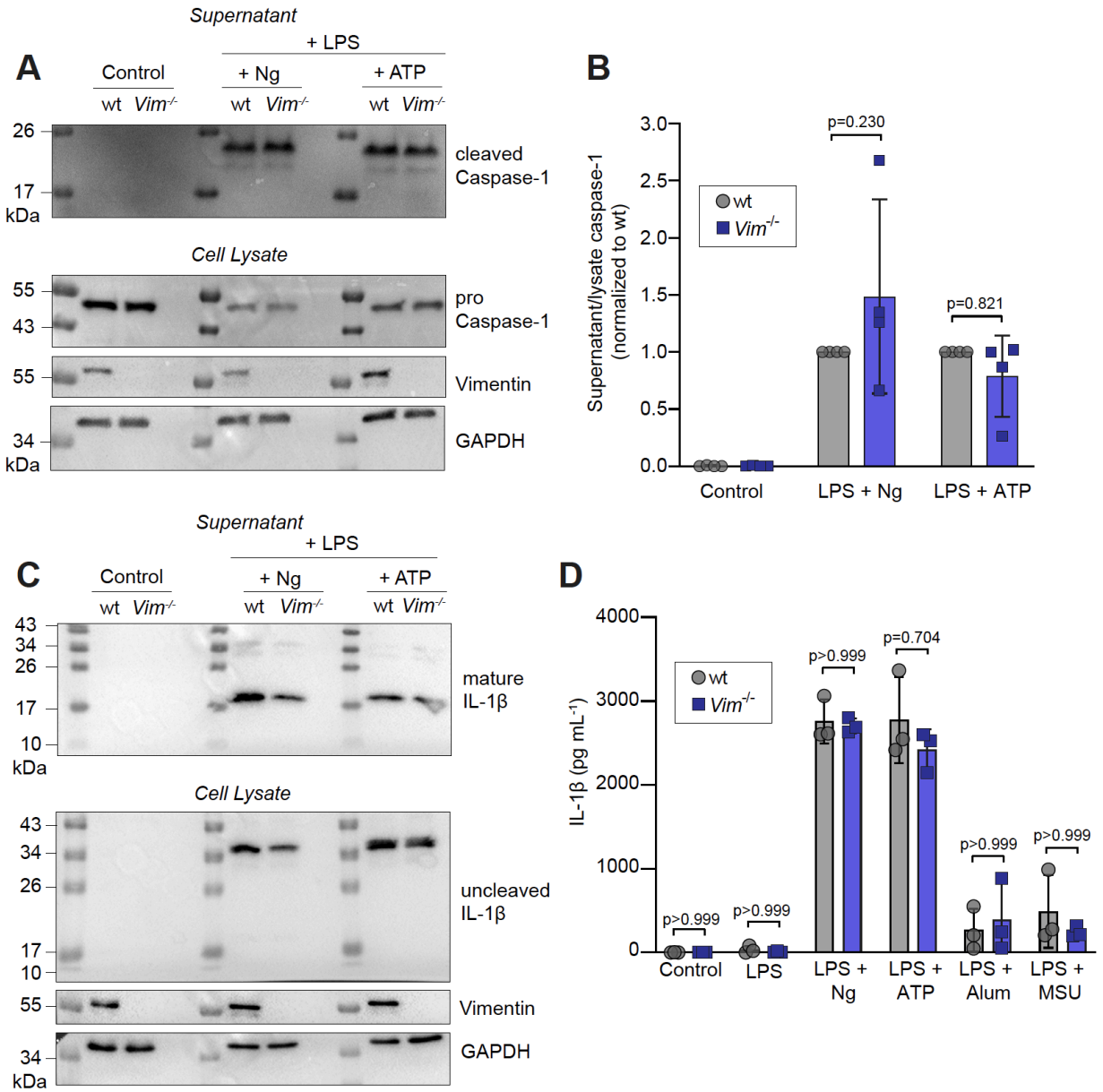

Figure 3. *Vim*$^{-/-}$ BMDM cleave and release caspase-1 and IL-1β following NLRP3 inflammasome activation. (A-C) LPS-primed (1 μg/mL, 4 h) BMDM were treated with nigericin (10 μM, 30 min) or ATP (3 mM, 1 h). Samples were visualized by SDS-PAGE against (A,B) uncleaved and cleaved capase-1, and C) immature and mature IL-1β. In B), quantification of the ratio of cleaved to uncleaved caspase-1 normalized to wt treatments is shown. Individual values ± SD (N=4). (D) Extracellular IL-1β measured in LPS-primed wt and *Vim*$^{-/-}$ BMDM treated with nigericin (10 μM) for 30 min, ATP (3 mM) for 1 h, alum (100 μg/ml) for 6 h, or MSU (100 μg/ml) for 16 h. Mature IL-1β concentration was measured by ELISA. Data represented as replicate means ± SD (minimum N=3).

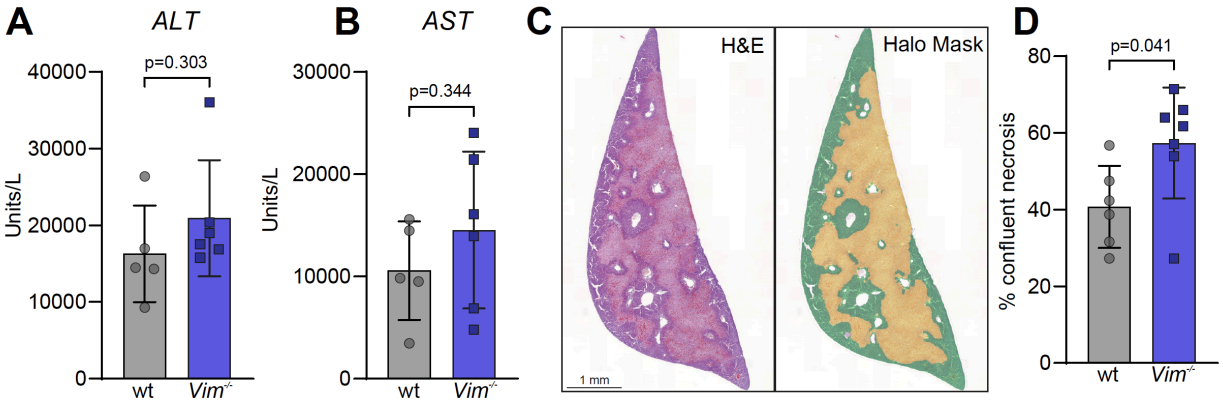

Figure 4. *Vim*$^{-/-}$ mice are not ostensibly protected against hepatic ischemia/reperfusion injury. Warm ischemia/reperfusion injury was modeled using male wt (C57Bl/6) control and *Vim*$^{-/-}$ mice between 6-12 weeks of age. (A,B) Levels of aspartate aminotransferase (AST) and alanine aminotransferase (ALT) in the serum of mice are graphed. (wt N=5, Vim$^{-/-}$ N=6 mice per group.) (C) Hematoxylin and eosin (H&E) staining of liver tissue samples along with Halo DenseNetV2 mask to detect healthy and necrotic areas. (D) Quantification of percent necrosis of liver samples (wt N=6, Vim$^{-/-}$ N=7 mice per group). All data shown as biological replicates ± SD.

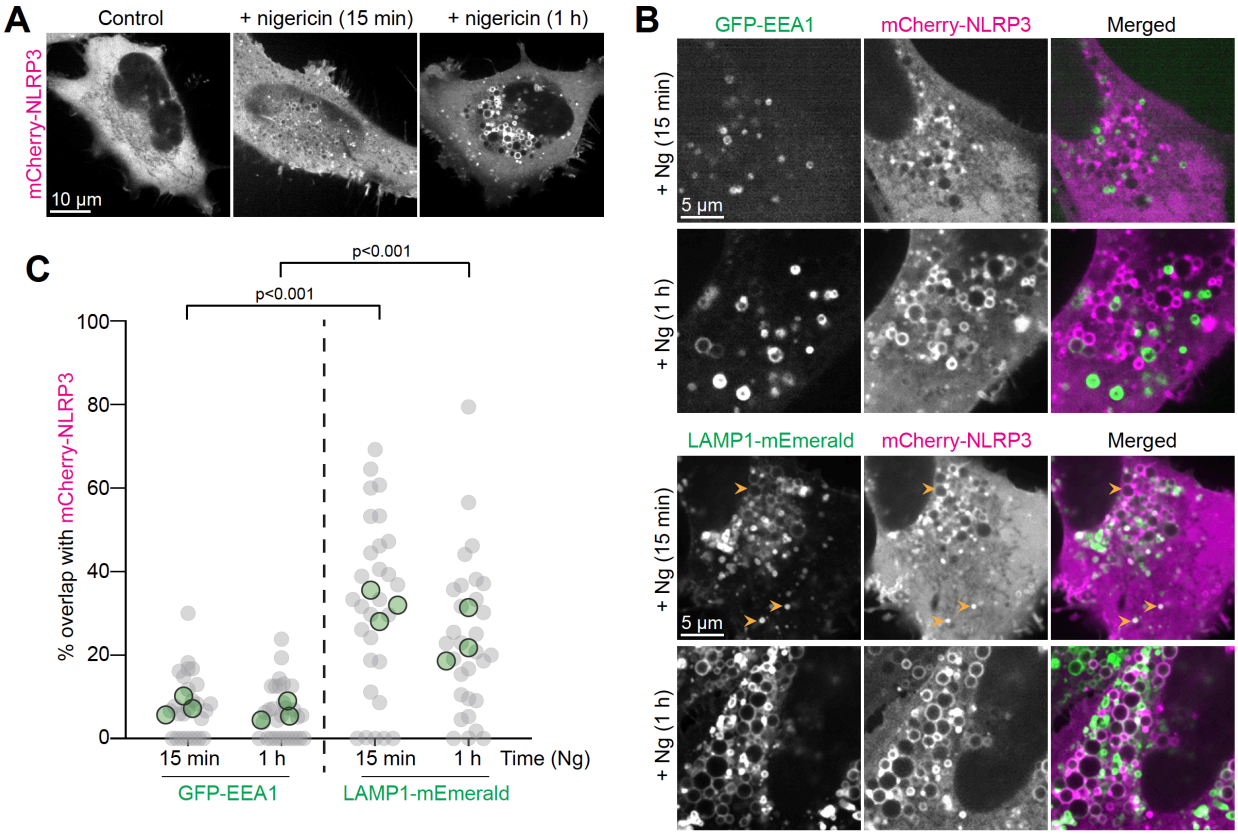

Figure 5. NLRP3 aggregates on LAMP1-positive vesicular compartments. (A) HeLa cells expressing mCherry-NLRP3 before and after treatment with nigericin (10 µM, 15 min and 1h). (B) Co-expression of mCherry-NLRP3 with GFP-EEA1 or LAMP1-mEmerald in nigericin-treated cells after 15 min or 1 h. (C) SODA analysis for object association. Data represented as distribution of percent NLRP3 objects coupled with EEA1- or LAMP1-positive objects. (N=3, with 5-10 cells per technical replicate). Data shown as replicate means and individual technical replicate values.

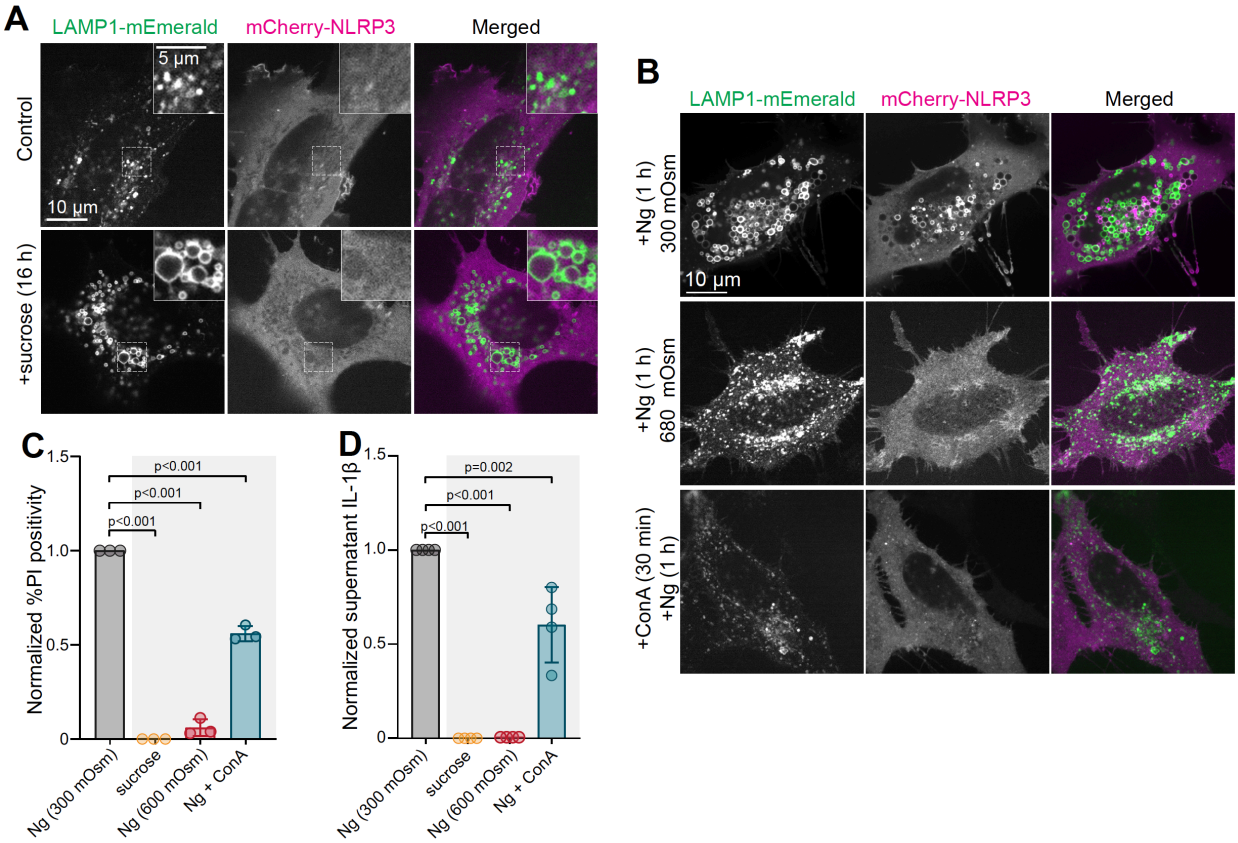

Figure 6. NLRP3 recruitment and activation are dependent on the activity of the V-ATPase. (A) HeLa cells co-expressing mCherry-NLRP3 and LAMP1-mEmerald following treatment with either nigericin (10 µM, 1 h) or sucrose (30 mM, 16 h). (B) HeLa cells co-expressing LAMP1-mEmerald and mCherry-NLRP3 treated with nigericin in either isotonic (300 mOsm) or hypertonic (680 mOsm) medium, or pre-treated with concanamycin A (1 µM, 30 min) prior to nigericin treatment in isotonic medium. (C, D) LPS-primed BMDM treated with nigericin (10 µM, 30 min), sucrose, or concanamycin A (1 µM, 30 min) followed by nigericin. In C), the percent PI positive cells normalized to LPS + nigericin treatment is shown (N=3). In D) the release of IL-1β measured by ELISA and normalized to LPS + nigericin treatment is shown (N=4). All data shown as individual replicate values ± SD.

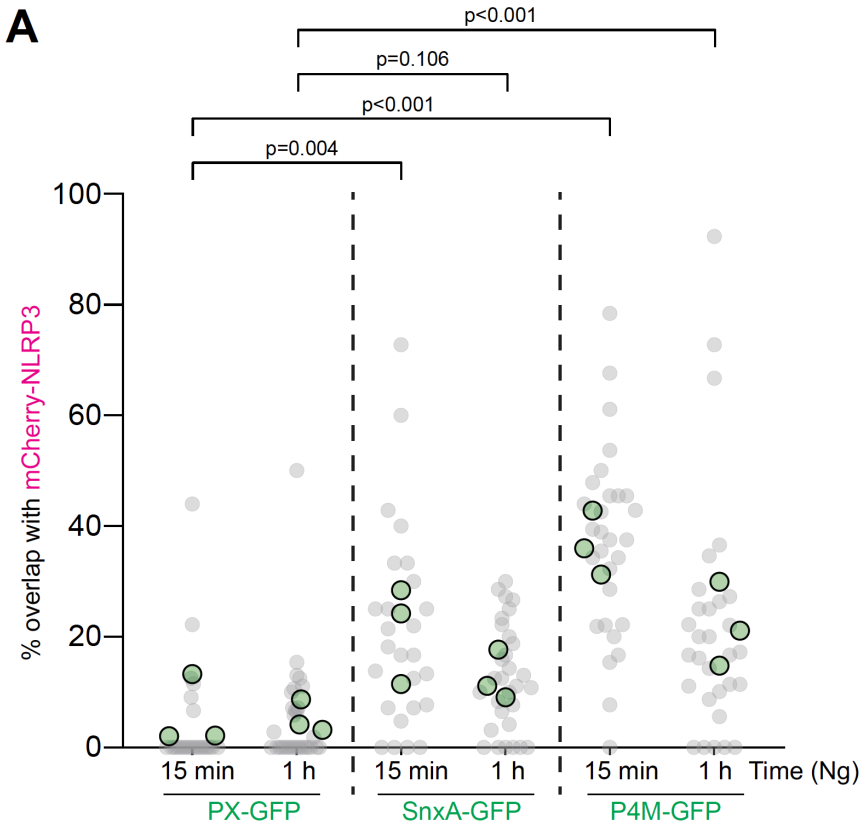

Supplemental Figure 1. NLRP3 associates with PI4P- and PI(3,5)P_2-positive vesicles following nigericin treatment. (A) SODA analysis for object association between NLRP3-mCherry and PX-GFP, SnxA-GFP, or GFP-P4M phosphoinositide probes following nigericin treatment (10 μM, 15 min and 1h). Data represented as distribution of percent NLRP3 objects coupled with phosphoinositide probe objects. (N=3, with 5-10 cells per technical replicate). All data shown as replicate means and individual technical replicate values.

613 **References**

614 Barberis, Laura, Christian Pasquali, Dominique Bertschy-Meier, Alessandra Cuccurullo, Carlotta
615 Costa, Chiara Ambrogio, Francis Vilbois, et al. 2009. "Leukocyte Transmigration Is
616 Modulated by Chemokine-Mediated PI3Kγ-Dependent Phosphorylation of Vimentin."
617 *European Journal of Immunology* 39 (4): 1136–46.
618 https://doi.org/10.1002/eji.200838884.
619 Battaglia, Rachel A., Samed Delic, Harald Herrmann, and Natasha T. Snider. 2018. "Vimentin on
620 the Move: New Developments in Cell Migration." *F1000Research* 7 (November):1796.
621 https://doi.org/10.12688/f1000research.15967.1.
622 Bauernfeind, Franz G., Gabor Horvath, Andrea Stutz, Emad S. Alnemri, Kelly MacDonald, David
623 Speert, Teresa Fernandes-Alnemri, et al. 2009. "Cutting Edge: NF-κB Activating Pattern
624 Recognition and Cytokine Receptors License NLRP3 Inflammasome Activation by
625 Regulating NLRP3 Expression." *The Journal of Immunology* 183 (2): 787–91.
626 https://doi.org/10.4049/jimmunol.0901363.
627 Brough, David, and Nancy J. Rothwell. 2007. "Caspase-1-Dependent Processing of pro-
628 Interleukin-1β Is Cytosolic and Precedes Cell Death." *Journal of Cell Science* 120 (5): 772–
629 81. https://doi.org/10.1242/jcs.03377.
630 Cai, Ruiqi, Ori Scott, Gang Ye, Trieu Le, Ekambir Saran, Whijin Kwon, Subothan Inpanathan, et al.
631 2024. "Pressure Sensing of Lysosomes Enables Control of TFEB Responses in
632 Macrophages." *Nature Cell Biology* 26 (8): 1247–60. https://doi.org/10.1038/s41556-
633 024-01459-y.
634 Chen, Jueqi, and Zhijian J. Chen. 2018. "PtdIns4P on Dispersed Trans-Golgi Network Mediates
635 NLRP3 Inflammasome Activation." *Nature* 564 (7734): 71–76.
636 https://doi.org/10.1038/s41586-018-0761-3.
637 Colucci-Guyon, Emma, Marie-Madeleine Portier, Irene Dunia, Denise Paulin, Sandrine Pournin,
638 and Charles Babinet. 1994. "Mice Lacking Vimentin Develop and Reproduce without an
639 Obvious Phenotype." *Cell* 79 (4): 679–94. https://doi.org/10.1016/0092-8674(94)90553-
640 3.
641 Costes, Sylvain V., Dirk Daelemans, Edward H. Cho, Zachary Dobbin, George Pavlakis, and
642 Stephen Lockett. 2004. "Automatic and Quantitative Measurement of Protein-Protein
643 Colocalization in Live Cells." *Biophysical Journal* 86 (6): 3993–4003.
644 https://doi.org/10.1529/biophysj.103.038422.
645 Eckes, B., E. Colucci-Guyon, H. Smola, S. Nodder, C. Babinet, T. Krieg, and P. Martin. 2000.
646 "Impaired Wound Healing in Embryonic and Adult Mice Lacking Vimentin." *Journal of*
647 *Cell Science* 113 (13): 2455–62. https://doi.org/10.1242/jcs.113.13.2455.
648 Evavold, Charles L., Jianbin Ruan, Yunhao Tan, Shiyu Xia, Hao Wu, and Jonathan C. Kagan. 2018.
649 "The Pore-Forming Protein Gasdermin D Regulates Interleukin-1 Secretion from Living
650 Macrophages." *Immunity* 48 (1): 35-44.e6.
651 https://doi.org/10.1016/j.immuni.2017.11.013.
652 Fang, Run, Qifei Jiang, Xinying Jia, and Zhengfan Jiang. 2023. "ARMH3-Mediated Recruitment of
653 PI4KB Directs Golgi-to-Endosome Trafficking and Activation of the Antiviral Effector
654 STING." *Immunity* 56 (3): 500-515.e6. https://doi.org/10.1016/j.immuni.2023.02.004.

655 Fink, Susan L., and Brad T. Cookson. 2006. “Caspase-1-Dependent Pore Formation during
656 Pyroptosis Leads to Osmotic Lysis of Infected Host Macrophages.” *Cellular Microbiology*
657 8 (11): 1812–25. https://doi.org/10.1111/j.1462-5822.2006.00751.x.
658 Franchi, Luigi, and Gabriel Núñez. 2008. “The Nlrp3 Inflammasome Is Critical for Aluminium
659 Hydroxide-Mediated IL-1β Secretion but Dispensable for Adjuvant Activity.” *European*
660 *Journal of Immunology* 38 (8): 2085–89. https://doi.org/10.1002/eji.200838549.
661 Greaney, Allison J., Stephen H. Leppla, and Mahtab Moayeri. 2015. “Bacterial Exotoxins and the
662 Inflammasome.” *Frontiers in Immunology* 6 (November).
663 https://doi.org/10.3389/fimmu.2015.00570.
664 Groß, Christina J., Ritu Mishra, Katharina S. Schneider, Guillaume Médard, Jennifer
665 Wettmarshausen, Daniela C. Dittlein, Hexin Shi, et al. 2016. “K + Efflux-Independent
666 NLRP3 Inflammasome Activation by Small Molecules Targeting Mitochondria.” *Immunity*
667 45 (4): 761–73. https://doi.org/10.1016/j.immuni.2016.08.010.
668 Hari, Aswin, Yifei Zhang, Zhongyuan Tu, Pascal Detampel, Melanie Stenner, Anutosh Ganguly,
669 and Yan Shi. 2014. “Activation of NLRP3 Inflammasome by Crystalline Structures via Cell
670 Surface Contact.” *Scientific Reports* 4 (1): 7281. https://doi.org/10.1038/srep07281.
671 Håversen, Liliana, Jeanna Perman Sundelin, Adil Mardinoglu, Mikael Rutberg, Marcus Ståhlman,
672 Ulrika Wilhelmsson, Lillemor Mattsson Hultén, et al. 2018. “Vimentin Deficiency in
673 Macrophages Induces Increased Oxidative Stress and Vascular Inflammation but
674 Attenuates Atherosclerosis in Mice.” *Scientific Reports* 8 (1): 16973.
675 https://doi.org/10.1038/s41598-018-34659-2.
676 He, Wan-ting, Haoqiang Wan, Lichen Hu, Pengda Chen, Xin Wang, Zhe Huang, Zhang-Hua Yang,
677 Chuan-Qi Zhong, and Jiahuai Han. 2015. “Gasdermin D Is an Executor of Pyroptosis and
678 Required for Interleukin-1β Secretion.” *Cell Research* 25 (12): 1285–98.
679 https://doi.org/10.1038/cr.2015.139.
680 Hohmann, Stefan. 2002. “Osmotic Stress Signaling and Osmoadaptation in Yeasts.” *Microbiology*
681 *and Molecular Biology Reviews* 66 (2): 300–372.
682 https://doi.org/10.1128/MMBR.66.2.300-372.2002.
683 Hornung, Veit, Franz Bauernfeind, Annett Halle, Eivind O Samstad, Hajime Kono, Kenneth L
684 Rock, Katherine A Fitzgerald, and Eicke Latz. 2008. “Silica Crystals and Aluminum Salts
685 Activate the NALP3 Inflammasome through Phagosomal Destabilization.” *Nature*
686 *Immunology* 9 (8): 847–56. https://doi.org/10.1038/ni.1631.
687 Ivaska, Johanna, Hanna-Mari Pallari, Jonna Nevo, and John E. Eriksson. 2007. “Novel Functions
688 of Vimentin in Cell Adhesion, Migration, and Signaling.” *Experimental Cell Research* 313
689 (10): 2050–62. https://doi.org/10.1016/j.yexcr.2007.03.040.
690 Jaeschke, Hartmut. 2003. “Molecular Mechanisms of Hepatic Ischemia-Reperfusion Injury and
691 Preconditioning.” *American Journal of Physiology-Gastrointestinal and Liver Physiology*
692 284 (1): G15–26. https://doi.org/10.1152/ajpgi.00342.2002.
693 Jiang, Susan X., Jacqueline Slinn, Amy Aylsworth, and Sheng T. Hou. 2012. “Vimentin Participates
694 in Microglia Activation and Neurotoxicity in Cerebral Ischemia: Vimentin Controls
695 Microglia Activation.” *Journal of Neurochemistry* 122 (4): 764–74.
696 https://doi.org/10.1111/j.1471-4159.2012.07823.x.

697 Jiménez-Castro, Mónica B., María Eugenia Cornide-Petronio, Jordi Gracia-Sancho, and Carmen
698 Peralta. 2019. "Inflammasome-Mediated Inflammation in Liver Ischemia-Reperfusion
699 Injury." *Cells* 8 (10): 1131. https://doi.org/10.3390/cells8101131.
700 Lagache, Thibault, Alexandre Grassart, Stéphane Dallongeville, Orestis Faklaris, Nathalie
701 Sauvonnet, Alexandre Dufour, Lydia Danglot, and Jean-Christophe Olivo-Marin. 2018.
702 "Mapping Molecular Assemblies with Fluorescence Microscopy and Object-Based Spatial
703 Statistics." *Nature Communications* 9 (1): 698. https://doi.org/10.1038/s41467-018-
704 03053-x.
705 Laliberte, Ronald E., James Eggler, and Christopher A. Gabel. 1999. "ATP Treatment of Human
706 Monocytes Promotes Caspase-1 Maturation and Externalization." *Journal of Biological*
707 *Chemistry* 274 (52): 36944–51. https://doi.org/10.1074/jbc.274.52.36944.
708 Lang, Florian, Gillian L. Busch, Markus Ritter, Harald Völkl, Siegfried Waldegger, Erich Gulbins,
709 and Dieter Häussinger. 1998. "Functional Significance of Cell Volume Regulatory
710 Mechanisms." *Physiological Reviews* 78 (1): 247–306.
711 https://doi.org/10.1152/physrev.1998.78.1.247.
712 Lee, Bali, Christopher Hoyle, Rose Wellens, Jack P. Green, Fatima Martin-Sanchez, Daniel M.
713 Williams, Billie J. Matchett, et al. 2023. "Disruptions in Endocytic Traffic Contribute to the
714 Activation of the NLRP3 Inflammasome." *Science Signaling* 16 (773): eabm7134.
715 https://doi.org/10.1126/scisignal.abm7134.
716 Li, Hanfen, Stephen B. Willingham, Jenny P.-Y. Ting, and Fabio Re. 2008. "Cutting Edge:
717 Inflammasome Activation by Alum and Alum's Adjuvant Effect Are Mediated by NLRP3."
718 *Journal of Immunology (Baltimore, Md.: 1950)* 181 (1): 17–21.
719 https://doi.org/10.4049/jimmunol.181.1.17.
720 Li, Hao, Yanling Guan, Bo Liang, Peng Ding, Xin Hou, Wei Wei, and Yang Ma. 2022. "Therapeutic
721 Potential of MCC950, a Specific Inhibitor of NLRP3 Inflammasome." *European Journal of*
722 *Pharmacology* 928 (August):175091. https://doi.org/10.1016/j.ejphar.2022.175091.
723 Li, Wujun, Dong Li, Liankang Sun, Zeyu Li, Liang Yu, and Shengli Wu. 2018. "The Protective
724 Effects of Estrogen on Hepatic Ischemia-Reperfusion Injury in Rats by Downregulating
725 the Ang II/AT1R Pathway." *Biochemical and Biophysical Research Communications* 503
726 (4): 2543–48. https://doi.org/10.1016/j.bbrc.2018.07.013.
727 Luteijn, Rutger D., Sypke R. Van Terwisga, Jill E. Ver Eecke, Liberty Onia, Shivam A. Zaver, Joshua
728 J. Woodward, Richard W. Wubbolts, David H. Raulet, and Frank J. M. Van Kuppeveld.
729 2024. "The Activation of the Adaptor Protein STING Depends on Its Interactions with the
730 Phospholipid PI4P." *Science Signaling* 17 (827): eade3643.
731 https://doi.org/10.1126/scisignal.ade3643.
732 Man, Si Ming, Lee J. Hopkins, Eileen Nugent, Susan Cox, Ivo M. Glück, Panagiotis Tourlomousis,
733 John A. Wright, Pietro Cicuta, Tom P. Monie, and Clare E. Bryant. 2014. "Inflammasome
734 Activation Causes Dual Recruitment of NLRC4 and NLRP3 to the Same Macromolecular
735 Complex." *Proceedings of the National Academy of Sciences* 111 (20): 7403–8.
736 https://doi.org/10.1073/pnas.1402911111.
737 Mangan, Matthew S.J., Anil Akbal, Sophie Rivara, Agnes Schröder, Gabor Horvath, Philipp Walch,
738 Jan Hegermann, et al. 2024. "Cytosolic Sodium Accumulation Is a Common Danger Signal
739 Triggering Endocytic Dysfunction and NLRP3 Inflammasome Activation."
740 https://doi.org/10.1101/2024.03.26.586774.

741 Martinon, Fabio, Virginie Pétrilli, Annick Mayor, Aubry Tardivel, and Jürg Tschopp. 2006. "Gout-
742 Associated Uric Acid Crystals Activate the NALP3 Inflammasome." *Nature* 440 (7081):
743 237–41. https://doi.org/10.1038/nature04516.
744 Mor-Vaknin, Nirit, Maureen Legendre, Yue Yu, Carlos H. C. Serezani, Sanjay K. Garg, Anna Jatzek,
745 Michael D. Swanson, et al. 2013. "Murine Colitis Is Mediated by Vimentin." *Scientific*
746 *Reports* 3 (1): 1045. https://doi.org/10.1038/srep01045.
747 Muñoz-Planillo, Raúl, Peter Kuffa, Giovanny Martínez-Colón, Brenna L. Smith, Thekkelnaycke M.
748 Rajendiran, and Gabriel Núñez. 2013. "K+ Efflux Is the Common Trigger of NLRP3
749 Inflammasome Activation by Bacterial Toxins and Particulate Matter." *Immunity* 38 (6):
750 1142–53. https://doi.org/10.1016/j.immuni.2013.05.016.
751 Nieminen, Mikko, Tiina Henttinen, Marika Merinen, Fumiko Marttila–Ichihara, John E. Eriksson,
752 and Sirpa Jalkanen. 2006. "Vimentin Function in Lymphocyte Adhesion and Transcellular
753 Migration." *Nature Cell Biology* 8 (2): 156–62. https://doi.org/10.1038/ncb1355.
754 Ostadal, B., Z. Drahota, J. Houstek, M. Milerova, I. Ostadalova, M. Hlavackova, and F. Kolar. 2019.
755 "Developmental and Sex Differences in Cardiac Tolerance to Ischemia–Reperfusion
756 Injury: The Role of Mitochondria." *Canadian Journal of Physiology and Pharmacology* 97
757 (9): 808–14. https://doi.org/10.1139/cjpp-2019-0060.
758 Pelegrin, Pablo, and Annmarie Surprenant. 2006. "Pannexin-1 Mediates Large Pore Formation
759 and Interleukin-1β Release by the ATP-Gated P2X7 Receptor." *The EMBO Journal* 25 (21):
760 5071–82. https://doi.org/10.1038/sj.emboj.7601378.
761 Perregaux, D., and C. A. Gabel. 1994. "Interleukin-1 Beta Maturation and Release in Response to
762 ATP and Nigericin. Evidence That Potassium Depletion Mediated by These Agents Is a
763 Necessary and Common Feature of Their Activity." *The Journal of Biological Chemistry*
764 269 (21): 15195–203.
765 Santos, Gimena dos, Micah R. Rogel, Margaret A. Baker, James R. Troken, Daniela Urich, Luisa
766 Morales-Nebreda, Joseph A. Sennello, et al. 2015. "Vimentin Regulates Activation of the
767 NLRP3 Inflammasome." *Nature Communications* 6 (1): 6574.
768 https://doi.org/10.1038/ncomms7574.
769 Schmacke, Niklas A., Fionan O'Duill, Moritz M. Gaidt, Inga Szymanska, Julia M. Kamper,
770 Jonathan L. Schmid-Burgk, Sophia C. Mädler, et al. 2022. "IKKβ Primes Inflammasome
771 Formation by Recruiting NLRP3 to the Trans-Golgi Network." *Immunity* 55 (12): 2271-
772 2284.e7. https://doi.org/10.1016/j.immuni.2022.10.021.
773 Selzner, Nazia, Markus Selzner, Wolfram Jochum, and Pierre-Alain Clavien. 2003. "Ischemic
774 Preconditioning Protects the Steatotic Mouse Liver against Reperfusion Injury: An ATP
775 Dependent Mechanism." *Journal of Hepatology* 39 (1): 55–61.
776 https://doi.org/10.1016/S0168-8278(03)00147-8.
777 Tan, Julie, and Julie A. Brill. 2014. "Cinderella Story: PI4P Goes from Precursor to Key Signaling
778 Molecule." *Critical Reviews in Biochemistry and Molecular Biology* 49 (1): 33–58.
779 https://doi.org/10.3109/10409238.2013.853024.
780 Volchuk, Allen, Anna Ye, Leon Chi, Benjamin E. Steinberg, and Neil M. Goldenberg. 2020.
781 "Indirect Regulation of HMGB1 Release by Gasdermin D." *Nature Communications* 11
782 (1): 4561. https://doi.org/10.1038/s41467-020-18443-3.
783 Wu, Tong, Cheng Zhang, Tianfeng Shao, Jianzhong Chen, and Diyu Chen. 2022. "The Role of
784 NLRP3 Inflammasome Activation Pathway of Hepatic Macrophages in Liver Ischemia–

785 Reperfusion Injury." *Frontiers in Immunology* 13 (June):905423.
786 https://doi.org/10.3389/fimmu.2022.905423.
787 Zhang, Zhirong, Rossella Venditti, Li Ran, Zengzhen Liu, Karl Vivot, Annette Schürmann, Juan S.
788 Bonifacino, Maria Antonietta De Matteis, and Romeo Ricci. 2023. "Distinct Changes in
789 Endosomal Composition Promote NLRP3 Inflammasome Activation." *Nature*
790 *Immunology* 24 (1): 30–41. https://doi.org/10.1038/s41590-022-01355-3.
791 Zhu, Ping, Lihua Duan, Jie Chen, Ali Xiong, Qin Xu, Hongwei Zhang, Fang Zheng, Zheng Tan, Feili
792 Gong, and Min Fang. 2011. "Gene Silencing of NALP3 Protects Against Liver Ischemia–
793 Reperfusion Injury in Mice." *Human Gene Therapy* 22 (7): 853–64.
794 https://doi.org/10.1089/hum.2010.145.
795